Dalton Transactions

ARTICLE

Luminescence thermometry in a Dy_4 single molecule magnet

Julio Corredoira-Vázquez,[a] Cristina González-Barreira, Matilde Fondo,[a,*] Ana M. García-Deibe,[a] Jesús Sanmartín-Matalobos,[a] Miguel A. Hernández-Rodríguez,[b] Luís D. Carlos[b,*]

Received 00th January 20xx,
Accepted 00th January 20xx

DOI: 10.1039/x0xx00000x

www.rsc.org/

The tetranuclear linear complex $[Dy_4(1,1,4\text{-}H_3L^r)_2(OAc)_6]\cdot CH_3OH$ (**1**·CH_3OH) was satisfactorily prepared and characterized. Its X-ray structure shows that it contains two types of octacoordinated Dy^{III} ions, with distorted triangular dodecahedral and square antiprism geometries. This complex is an SMM, with multiple relaxation pathways, and with an anisotropic energy barrier of 39.7 K. **1**·CH_3OH also operates as a luminescent thermometer in the 11–295 K range with a maximum relative thermal sensitivity of 1.6%·K^{-1} and a minimum temperature uncertainty of 1.1 K, both values at 295 K. Thus, **1**·CH_3OH is the first Dy_4 SMM with luminescent thermometry, and this system is a rare example of dysprosium SMM that accesses the thermometric characteristics involving the ligand ascribed to the triplet emission in combination with Dy^{III} emission.

Introduction

The fabrication of electronic devices at the atomic and nanoscale remains an exciting technological challenge. The creation of such devices is spurred by a growing need for faster, lower-power electronics, and higher-density, higher-speed data storage. In this regard, one promising area is that of molecule magnets.[1,2] Lanthanoid based nanomagnets have demonstrated to be the best single molecule magnets performers so far. Among them, according to the theory of Long et al,[3] the dysprosium complexes in a pseudolinear environment have been the ones that have reached the highest blocking temperatures.[4,5] Thus, the current record blocking temperature (T_B) of 80 K was set in 2018 with a pseudolinear Dy^{III} SIM.[5] Recently, a new dinuclear dysprosium complex equalled this record.[6] But one of the important problems with these magnets of T_B greater than the temperature of liquid nitrogen is their instability in air. Therefore, many challenges still remain in the field of molecular magnets. The first of these is the development of air-stable single-molecule magnets (SMMs) with higher operating temperatures. But a second major challenge is to control the temperature of these nanomagnets, since excessive heating could cause them to lose their behaviour as such. Unfortunately, temperature measurement in the sub-micrometre spatial range is not possible with conventional contact thermometers. One way to overcome this impasse is to build microdevices with materials capable of also acting as in-situ thermometers. In this sense, there are some very recent publications that try to provide solutions for the measurement of temperature in molecular magnets, making use of luminescent thermometry,[7-17] and some of the achievements were summarised by Murugesu and colaborators.[18] Among these works, most studies have been carried out with homodinuclear compounds of Dy^{III},[7b] Tb^{III},[7c] or Yb^{III}.[7a] However, some examples of heteronuclear $Yb^{III}Co^{III}$,[9,14] $Dy^{III}Co^{III}$,[15] or $[Ho^{III}_xY_{1-x}]M^{III}$ (M = Co, Rh or Ir) compounds[16] have also been described, in addition to some mononuclear complexes. Thus, some of us have published the first mononuclear Yb^{III} compound with slow relaxation of magnetization and luminescent thermometry,[10] which currently accompanies other two complexes of the same metal.[13] Additionally, some other mononuclear dysprosium compounds have been published,[11,12,17] as well as a mononuclear Nd^{III} complex,[8] which combine their character as single ion magnets (SIMs) and their luminescent thermometric capacity. Accordingly, the field of the SMMs as luminescent thermometers is still in its beginnings.

With these considerations in mind, in this paper we describe the SMM behaviour, and analyse the luminescent thermometer properties of a tetranuclear dysprosium compound.

Experimental

Materials and general methods

All chemical reagents were purchased from commercial sources, and used as received without further purification. Elemental analyses of C, H and N were performed on a Themoscientific Flash Smart analyser.

Syntheses

The ligand used in this work was obtained from reduction of the previously prepared H_3L Schiff base (Scheme 1),[19] using a variation of a described method,[20] as formerly reported by us,[10] and satisfactorily characterised according to published results.[10,20]

$[Dy_4(1,1,4\text{-}H_3L^r)_2(OAc)_6]\cdot CH_3OH$ (1·CH_3OH): A solution of $Dy(OAc)_3$ (0.135 g, 0.397 mmol) in methanol (25 mL) was added to a solution of a mixture of 1,2,4-$H_6L_c^r$ and 1,1,4-$H_6L_c^r$ (0.100 g, 0.198 mmol) in chloroform (20 mL). The mixture was stirred at room

[a] *Departamento de Química Inorgánica, Facultade de Química, Universidade de Santiago de Compostela, 15782 Santiago de Compostela, Spain E-mail: matilde.fondo@usc.es.*
[b] *Phantom-g, CICECO – Aveiro Institute of Materials, Department of Physics, University of Aveiro, 3810-193 – Aveiro, Portugal*
[c] *Electronic Supplementary Information (ESI) available: Tables S1-S3 and Figures S1-S5. CCDC 2184024 (**1**·CH_3OH). For ESI and crystallographic data in CIF format see DOI: 10.1039/x0xx00000x.*

temperature for 12 h, and subsequently concentrated up to 1/3 of its volume. The slow evaporation of this concentrated solution yielded single crystals of $[Dy_4(1,1,4\text{-}H_3L^r)_2(OAc)_6]\cdot CH_3OH$ (**1**·CH_3OH), suitable for X-ray diffraction studies. The crystals were filtered and dried in the vacuum line. Yield: 0.06 g (31 %). Elemental analysis calcd. for $C_{67}H_{88}Dy_4N_8O_{19}$ (1947.36): C 41.07, N 5.72, H 4.53 %. Found: C 40.86, N 5.61, H 4.55 %.

Single X-ray crystallographic refinement and structure solution

Crystal data and details of refinement are given in Table S1. The single crystals of **1**·CH_3OH could be obtained as detailed above. Data were collected at 100 K on a Bruker D8 VENTURE PHOTON III-14 diffractometer, employing graphite monochromatised Mo-$K\alpha$ (λ = 0.71073 Å) radiation. Multi-scan absorption corrections were applied using the SADABS routine.[21] The structure was solved by standard direct methods employing SHELXT,[22] and then refined by full matrix least-squares techniques on F^2 by using SHELXL, from the program package SHELX-2018.[22] All atoms different from hydrogen were anisotropically refined, while H atoms were typically included in the structure factor calculations in geometrically idealised positions. However, with the intention of revealing the hydrogen bonding scheme, hydrogen atoms attached to amine nitrogen atoms were located in the corresponding Fourier map. In this case, either they were freely refined, or with thermal parameters derived from their parent atoms.

Powder X-ray diffraction studies

The powder diffractogram for **1**·CH_3OH was recorded on a Philips diffractometer with a control unity type "PW1710", a vertical goniometer type "PW1820/00" and a generator type "Enraf Nonius FR590", operating at 40 kV and 30 mA, using monochromated Cu-Kα (λ = 1.5418 Å) radiation. A scan was performed in the range 2 < 2θ < 50° with t = 3 s and Δ2θ = 0.02°. LeBail refinement was obtained with the aid of HighScore Plus Version 3.0d.

Magnetic measurements

Magnetic susceptibility *dc* and *ac* measurements for a microcrystalline sample of **1**·CH_3OH were carried out with a PPMS Quantum Design susceptometer. The crystals were ground, and 18.704 mg of the microcrystalline powder were delivered inside a pollycarbonate capsule, and this was introduced in the susceptometer.

The *dc* magnetic susceptibility data were recorded under a magnetic field of 1000 Oe in the temperature range 2–300 K. Magnetisation measurements at 2.0 K were recorded under magnetic fields ranging from 0 to 70000 Oe. Diamagnetic corrections were estimated from Pascal's Tables. Alternating current (*ac*) susceptibility measurements at zero *dc* field were performed with an oscillating *ac* field of 3.5 Oe, and *ac* frequencies ranging from 10 to 10000 Hz in the 2-25 K temperature range. *ac* measurements at 3 K were also recorded under magnetic fields of 250, 500, 750, 1000, 1500 and 2000 Oe, with an oscillating *ac* field of 3.5 Oe, and *ac* frequencies ranging from 50 to 1500 Hz.

Luminescence measurements

The temperature-dependent emission and excitation spectra in solid state for **1**·CH_3OH were recorded using a Fluorolog3® Horiba Scientific (Model FL3-2T) spectroscope, with a modular double grating excitation spectrometer (fitted with a 1200 grooves/mm grating blazed at 330 nm) and a TRIAX 320 single emission monochromator (fitted with a 1200 grooves/mm grating blazed at 500 nm, reciprocal linear density of 2.6 nm mm^{-1}), coupled with an R298 Hamamatsu photomultiplier, using the front face acquisition mode. The excitation source was a 450 W Xe arc lamp. The emission spectra were corrected for detection and optical spectral response of the spectrofluorimeter, and the excitation spectra were corrected for the spectral distribution of the lamp intensity using a photodiode reference detector. The temperature was controlled by a helium-closed cycle cryostat, a vacuum system (4×10^{-4} Pa), and an autotuning temperature controller (Lakeshore 330, Lakeshore) with a resistance heater. The temperature was measured by a silicon diode cryogenic sensor (DT-470-SD, Lakeshore) with an accuracy of ±0.5 K (12–30 K), ±0.25 K (30–60 K), and ±0.15 K (60–340 K).

Absorption spectrum of **1**·CH_3OH in methanol solution was recorded on a JASCO V-630 spectrophotometer, and solution fluorescence emission spectra on a JASCO FP-8300 spectrofluorimeter. The linearity of the fluorescence emission versus concentration was checked in the concentration range used (10^{-4}–10^{-6} M). The correction of the absorbed light was performed when considered necessary. The spectrophotometric characterisation was made by preparing stock solutions of the free ligand and dysprosium acetate in methanol (10^{-3} M). The studied solutions were prepared by appropriate dilution of the stock solution up to 10^{-4}-10^{-6} M. All the measurements were taken at 298 K.

Thermometric analysis

The relative thermal sensitivity (S_r) of **1**·CH_3OH was estimated by:

$$S_r = \frac{1}{\Delta}\left|\frac{\partial \Delta}{\partial T}\right| \quad (1)$$

where Δ is the thermometric parameter and T the temperature (measured by the Si diode). Here, Δ is defined as the ratio between the integrated intensity of the ligand emission (I_1) and that of the Dy^{III} $^4F_{9/2}\rightarrow{}^6H_{13/2}$ transition. The temperature uncertainty (δT), which quantifies the temperature resolution[23]

$$\delta T = \frac{1}{S_r}\frac{\delta \Delta}{\Delta} \quad (2)$$

being $\delta\Delta/\Delta$ the relative uncertainty in Δ estimated through:

$$\frac{\delta \Delta}{\Delta} = \sqrt{\left(\frac{\delta I_1}{I_1}\right)^2 + \left(\frac{\delta I_2}{I_2}\right)^2} \quad (3)$$

where $\delta I_i/I_i$ (I = 1,2) is calculated dividing the readout fluctuations of the baseline by the maximum value of each intensity, i.e., I_1 and I_2.[23] As the integrated areas are calculated from the same emission spectra then $\delta I_1 = \delta I_2 = \delta I$. The S_r and δT parameters enable the comparison of the performance of the luminescent thermometer with that of similar sensors.

Results and discussion

Synthesis

The tetranuclear complex $[Dy_4(1,1,4\text{-}H_3L^r)_2(OAc)_6]\cdot CH_3OH$ (**1**·CH_3OH, with H_6L^r = 2,2',2''-(2,5,8,11-tetraazadodecane-1,1,12-triyl)triphenol) has been obtained from $Dy(OAc)_3$, and the isomeric

mixture of 1,1,4-$H_6L_c^r$ and 1,2,4-$H_6L_c^r$. This latter has been prepared as previously reported,[10,20] from the reduction of the corresponding Schiff base H_3L, as summarized in Scheme 1.

Accordingly, the reaction of the aminophenol isomers with the dysprosium salt in 1:1 molar ratio yields complex **1**·CH_3OH. The same compound, with improved yield, is isolated when the molar ratio increases to 2:1 (Scheme 1). **1**·CH_3OH is isolated from the mother solution in the form of single crystals, suitable for X-ray diffraction studies, and its crystal structure clearly shows that the complex contains the $[1,1,4\text{-}H_3L^r]^{3-}$ isomer, without trace of the $[1,2,4\text{-}H_3L^r]^{3-}$ one. This agrees with previous results,[10,17] which show that an increase on the pH of the medium, in this case by use of the acetate salt, displaces the equilibrium towards the $[1,1,4\text{-}H_3L^r]^{3-}$ species. Complex **1**·CH_3OH also shows the versatility of the chemistry with this kind of ligand as a function of the metal salt employed, given that the same reaction using dysprosium nitrate instead of dysprosium acetate yields the dinuclear SMM $[Dy(1,2,4\text{-}H_3L^r)]_2$,[24] where the anion of the metal salt is absent.

1·CH_3OH was fully characterised by analytical, and X-ray diffraction studies. The comparison of the experimental powder X-ray diffractogram of the final product with the calculated one from single X-ray diffraction data (Fig. S1) indicates that **1**·CH_3OH has been obtained with high purity, without mixtures, and that the collected sample and the solved single crystal are the same compound.

The magnetic and luminescent properties of **1**·CH_3OH were also investigated.

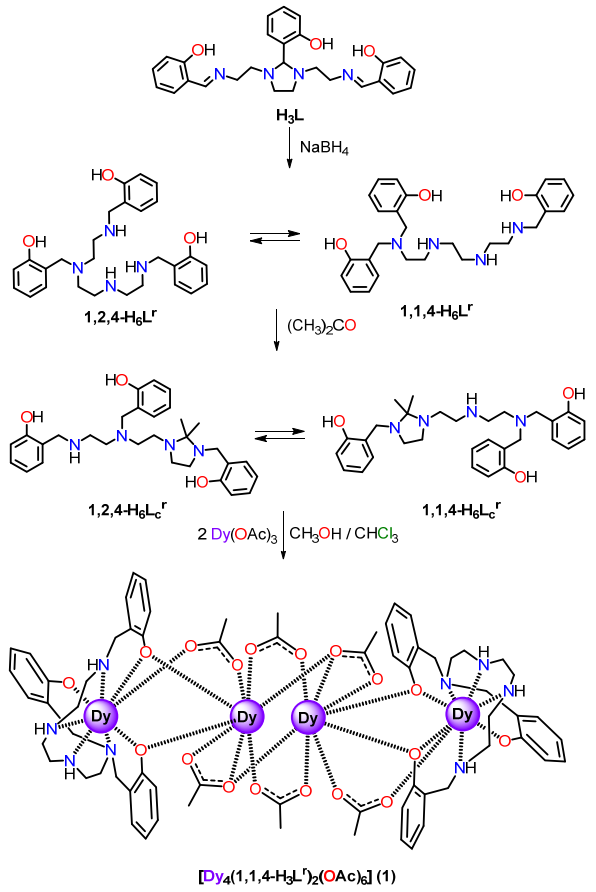

Scheme 1 Synthetic route for isolation of **1**.

X-ray diffraction studies

The unit cell of $[Dy_4(1,1,4\text{-}H_3L^r)_2(OAc)_6]\cdot CH_3OH$ (**1**·CH_3OH) contains linear tetranuclear $[Dy_4(1,1,4\text{-}H_3L^r)_2(OAc)_6]$ molecules, and methanol as solvate. An ellipsoid diagram for **1** is shown in Fig. 1, and main bond distances and angles in Table S2.

The $[Dy_4(1,1,4\text{-}H_3L^r)_2(OAc)_6]$ molecules have an inversion centre, which makes its halves equivalent. In this molecule, there are two clearly distinguishable types of Dy^{III} ions, and it can be understood as two $[Dy(1,1,4\text{-}H_3L^r)(OAc)]^-$ units that join a $[Dy_2(OAc)_4]^{2+}$ cation between them. Thus, in the $[Dy(1,1,4\text{-}H_3L^r)(OAc)]^-$ anion, the 1,1,4 isomer of the aminophenol acts as a trianionic heptadentate ligand, using all its nitrogen and oxygen atoms to bind the metal centre, as usual.[10,20,24] This provides an N_4O_3 environment around Dy1 (Scheme 1, Fig. 1). The coordination sphere of Dy1 is completed with an oxygen atom (O1) from an acetate ion, and SHAPE calculations[25] for the DyN_4O_4 core (Table S3) indicate that the geometry around the Dy^{III} centre is distorted triangular dodecahedral.

In the $[Dy_2(OAc)_4]^{2+}$ cation, the two dysprosium atoms, which are crystallographically equivalent, are bound by four acetate groups, two acting as μ_2-κ^1:κ^1 bridges in a *syn-syn* mode, and two as μ_2-κ^2:κ^1 bridges. This cation is joined to the $[Dy(1,1,4\text{-}H_3L^r)(OAc)]^-$ moieties, in such a way that the anion uses two phenoxy oxygen atoms from positions 1 and 4 of the aminophenol (O11 and O13), respectively, and one oxygen atom from the acetate group (O2) to bind Dy2. This leads to $(1,1,4\text{-}H_3L^r)^{3-}$ acting as a μ_2-κ^7:κ^2 ligand (Scheme 1, Fig. 1), a coordination mode that has not been described so far for this type of aminophenol,[10,20,24,26] and the acetate ligand, initially belonging to the anion, is now acting as a μ_2-κ^1:κ^1 bridge in a *syn-syn* mode.

The mentioned features lead to Dy2 in an O_8 environment, with a square antiprism geometry, distorted towards a triangular dodecahedron, according to SHAPE calculations (Table S3).

All the above characteristics mean that the four dysprosium atoms are in a basically linear arrangement, with Dy1···Dy2···Dy2 or Dy2···Dy2···Dy1 angles of 171.78(1)°. Between them, Dy1 and Dy2 are triple-bridged, by two $O_{phenoxide}$ atoms and one *syn- syn* acetate. This leads to Dy1···Dy2 distances of 3.7561(5) Å, with Dy1-O-Dy2 angles of *ca*. 107° (Table S2). Both Dy2 centres, as already mentioned, are quadruple bridged, by the four acetates, leading to intramolecular Dy2···Dy2 distances of 3.8274(6) Å, with Dy2-O5-Dy2 angles of 104.38(16)º. All other bond distances and angles are within the expected ranges,[10,20,24,26-28] and do not merit further discussion. However, it is worth noting that the Dy1-O12 distance, which corresponds to the bond between the dysprosium atom and the

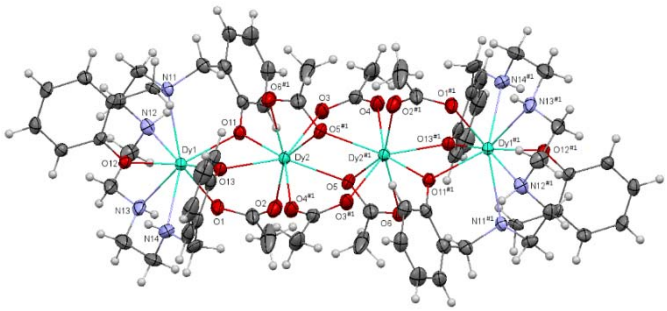

Fig. 1 Ellipsoid diagram (50 % probability) for **1**. The C and H atoms were not labelled, for clarity.

terminal phenoxy oxygen atom, is considerably shorter than any other Dy-O distance (Table S3).

Besides, the shortest intermolecular Dy···Dy distance is between the terminal Dy1 atoms of neighbouring units, and it is 8.8932(7) Å (Fig. S2).

Magnetic Properties

Direct-current (*dc*) magnetic susceptibility measurements were recorded for a microcrystalline powder sample of **1**·CH_3OH as a function of the temperature. The $\chi_M T$ *vs T* plot is shown in Fig. 2.

The $\chi_M T$ value at 300 K is 54.1 cm^3Kmol^{-1}, close to, but slightly lower than the expected one for four uncoupled Dy^{III} ions at room temperature (56.68 cm^3Kmol^{-1}), which could indicate a weak intramolecular antiferromagnetic coupling. This value remains practically constant till 80 K, and then the curve falls sharply to a $\chi_M T$ value of 25.4 cm^3Kmol^{-1} at 2 K. This drop in the curve could be mainly due to the depopulation of the M_J sublevels of the Dy^{III} ions, which arise from the splitting of the spin-orbit ground multiplet by the ligand field, but Zeeman effects, and possible intramolecular anti-ferromagnetic, or intermolecular dipolar interactions can also contribute.

The field dependence of the magnetisation at 2 K tends to 23.80 $N\mu_B$ at the maximum applied field of 7 T (Fig. 2, inset), value that is far away from the theoretical one initially anticipated for four isolated Dy^{III} ions (40 $N\mu_B$), but close to the value of 20 $N\mu_B$ for four highly anisotropic Dy^{III} ions (5 $N\mu_B$ per ion) with an Ising-like ground doublet.[29]

The dynamic magnetic properties of **1**·CH_3OH were also studied, showing that in the absence of a *dc* field, the out-of-phase (χ''_M, Fig. 3 and Fig. S3) signals of the *ac* susceptibility feature frequency- and temperature dependent phenomena, with peaks for χ''_M in the temperature range 3-17 K. This behaviour indicates that **1**·CH_3OH is an SMM, but the shape of χ''_M *vs T* curves (Fig. S3), which do not tend to zero at 2 K, agree with the presence of quantum tunnelling of the magnetisation (QTM).

Fitting the Cole–Cole plot to the generalised Debye model suggests the presence of more than one relaxation process (α parameters in the range 0.42-0.07, Fig. S4). The relaxation time (τ), and energy barrier for this SMM were extracted from the τ^{-1} versus *T* plot (Fig. 4). According to the experimental QTM observed, the α values, and the non-linear character of this plot (Fig. 4), it is clear that there is more than one relaxation process. Accordingly, we have tried to fit the τ^{-1} versus *T* curve taking into account all the possible relaxation processes (Direct, Orbach, Raman and/or QTM), individually or grouped. Nevertheless, the Direct process could already be ruled out in advance since the magnetic measurements have been carried out in the absence of external magnetic field. Thus, as expected, such a relaxation process does not seem to take place, and the best fit of the temperature dependence of the relaxation time curve is achieved by the equation 4, considering Orbach, Raman and QTM relaxation (Fig. 4 and S5).

$$\tau^{-1} = \tau_0{}^{-1} e^{-U_{eff}/k_B T} + CT^n + \tau_{QTM}{}^{-1} \quad (4)$$

This fit yields the parameters U_{eff} = 39.7 K (27.6 cm^{-1}), $\tau_0 = 3.9\times10^{-6}$ s, C = 4.0 s^{-1} K^{-n}, n = 3.1, and $\tau_{QTM} = 1.0\times10^{-3}$ s. The n value can seem quite low, but considerations of both the acoustic and optical phonons in magnetic dynamics can explain the deviation from the predicted value for the Kramers ion (n = 9).[30] The effective energy barrier for the spin reversal (U_{eff}) value is close to that found for other linear tetranuclear Dy^{III} complexes with oxo and/or carboxylate bridges,[31-35] but it is below the U_{eff} record for a linear Dy_4 complex with oxygen bridges, which is 173 K.[36]

Besides, as this fit indicates that QTM exists, attempts were made to eliminate this quantum channel in order to obtain more accurate Orbach and Raman parameters. Thus, new ac measurements were recorded under different external dc fields at 3 K (Fig. S6), with the aim of determining the optimum field. However, as it can be seen in Fig. S6, the application of an external dc field does not improve the magnetic results, and it seem that this external field is unable to destroy or reduce the QTM.

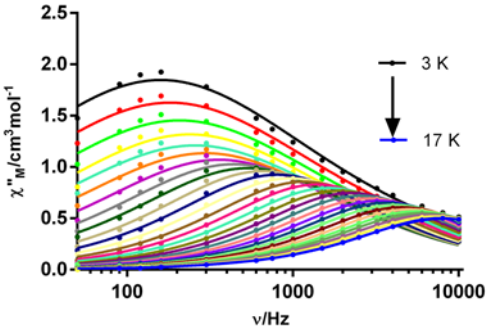

Fig. 3 Frequency dependence of χ''_M at different temperatures in a zero applied field for **1**·CH_3OH.

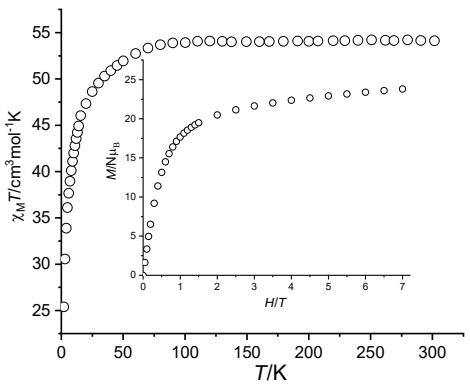

Fig. 2 $\chi_M T$ *vs T* for **1**·CH_3OH. Inset: $M/N\mu_B$ *vs H* at 2 K.

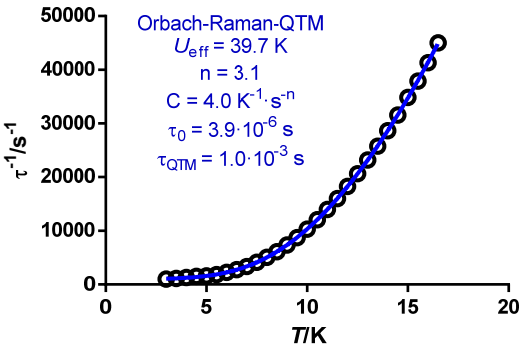

Fig. 4. τ^{-1} versus *T* plot for **1**·CH_3OH in zero field. The red solid line accounts for the best fit considering combined Orbach, Raman and QTM relaxation processes.

Luminescence studies

Fig. 5 shows the temperature dependence emission and excitation spectra of **1**·CH_3OH, recorded within the 11–295 K range. For all temperatures, the emission spectra are composed by a broadband ranging from 420 to 650 nm and ascribed to the ligand triplet state ($T_1 \rightarrow S_0$). The triplet nature of this emission is inferred by the time-resolved experiments of Fig. S7 showing an overall decrease of the intensity of the band increasing the starting delay from 0.05×10^{-3} to 0.15×10^{-3} s. The triplet nature of the ligand broadband emission of **1**·CH_3OH is also confirm by the absence of any transition in the 350–700 nm interval in the absorption spectrum of a similar ligand (see Fig. S8). In the analogue [Dy_2(bpm)(tfaa)$_6$] SMM, Errulat *et al*. also attributed a triplet nature to the ligand emission.[7b] The intensity of the broadband increases as the temperature decreases, and for temperatures below 200 K a sharp emission band around 577 nm related to the Dy^{III} $^4F_{9/2} \rightarrow {}^6H_{13/2}$ transition starts to be discerned (Fig. 5a).

On the other hand, the excitation spectra show an excitation broadband ranging from 280 to 420 nm for all temperatures. However, on this broadband, Dy^{III} related self-absorption transitions around 325 nm ($^6H_{15/2} \rightarrow {}^4K_{15/2}$), 351 nm ($^6H_{15/2} \rightarrow {}^4M_{15/2}$, $^4P_{7/2}$) and 364 nm ($^6H_{15/2} \rightarrow {}^4I_{15/2}$) can be observed, especially at lower temperatures (Fig. 5b). This reabsorption phenomenon, well-known in the literature as "inner filter effect",[37-39] is observed in **1**·CH_3OH because the Dy^{III} ions (the acceptors) have energy levels resonant with the emission of the ligand (the emitter) absorbing, therefore, part of its luminescence. As the temperature decreases, the overall intensity of the ligand excitation broadband and Dy^{III} related self-absorption transitions increase (see Fig. 5b).

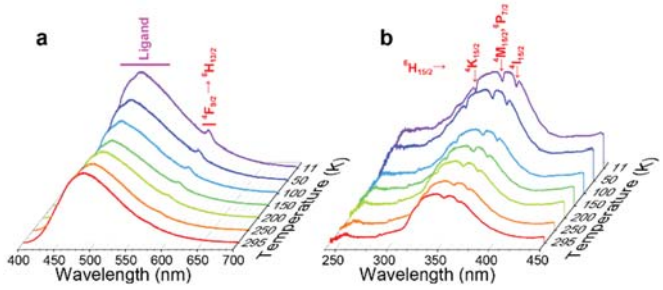

Fig. 5. Temperature dependence of the **1**·CH_3OH sample **(a)** emission spectra upon 358 nm excitation and **(b)** excitation spectra monitoring the emission band related to the $^4F_{9/2} \rightarrow {}^6H_{13/2}$ Dy^{III} transition at 577 nm.

A further observation of the temperature dependence of the emission spectra reveals that the ligand broadband and the $^4F_{9/2} \rightarrow {}^6H_{13/2}$ Dy^{III} transitions undergo different trends as the temperature increases from 11 to 295 K, Fig. 6. The integrated intensity of the Dy^{3+} intra-4f transitions was estimated considering the integration range between 560 and 590 nm without the contribution of the ligand emission that was removed with the proper subtraction of the background. The integrated intensity of the ligand, on the other hand, was estimated integrating the whole emission spectrum between 400 and 700 nm) and subtracting the abovementioned Dy^{3+} integrated intensity.

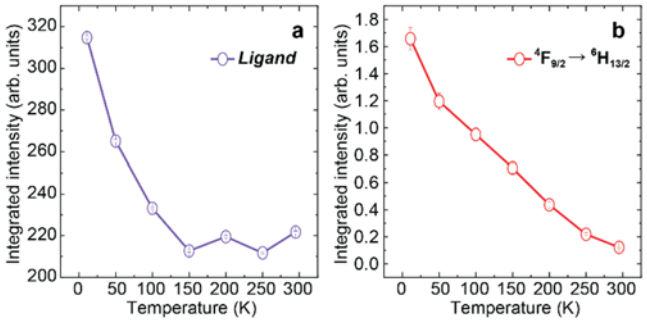

Fig. 6 Temperature dependence of the integrated intensities associated to the **(a)** ligand and **(b)** $^4F_{9/2} \rightarrow {}^6H_{13/2}$ related emission bands.

From the figure, it is evident that the ligand emission decreases as the temperature increases until reaching a plateau, from 150 K and beyond (Fig. 6a), whereas Dy^{III} emission monotonously decreases with the temperature (Fig. 6b). A similar trend with the temperature is observed for the Dy^{III} and ligand related excitation bands (Fig. S8).

Thermometric characterization

The different temperature behaviour exhibited by the ligand (I_1) and Dy^{III} (I_2) integrated intensities suggests that the intensity ratio I_1/I_2 is temperature-dependent and, therefore, it can be used as the thermometric parameter (Δ) to access the thermometric properties of **1**·CH_3OH. Fig. 7a shows the temperature evolution of Δ. From this figure, it can be observed that Δ exponentially increases with the

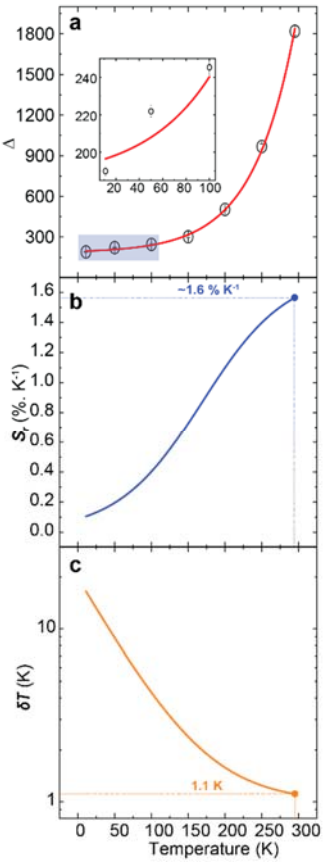

Fig. 7. (a) Temperature dependence of the thermometric parameter (Δ). The red curve represents a single exponential function as the best fit to the experimental data (r>0.99). Inset: zoomed region of Δ below 150 K. Temperature dependence of (b) the relative sensitivity, S_r and (c) the temperature uncertainty, δT.

Table 1. Excitation wavelength (λ, nm), temperature range (ΔT, K), maximum relative sensitivity (S_m, % K^{-1}), and corresponding temperature (T_m, K) of illustrative Dy^{III}-SMM luminescent thermometers.

Dy^{III}-SMM thermometer	λ	ΔT	Sm	T_m	Ref.
1·CH_3OH	358	11-295	1.6	295	This work
$[Dy(tba)_3phen]CH_2Cl_2$	320	10-50	1.1	50	17
$[Dy(acac)_3(H_2O)_2]\cdot H_2O$	364	5-290	5.4[a]	33	12
$[Dy(acac)_3(PyAm)]$	328	12-323	2.03[a]	12	11
$[Dy(acac)_3(PmAm)]$		12-340	0.76[a]	82	
$[Dy_2(bpm)(tfaa)_6]$	405	5.4-85.5	~1.8[b]	5.4	7b
	330	90-300	0.45[b]	90	
	330	298-398	3.3[c]	298	
$[DyCo(CN)_6(bpyO_2)_2(H_2O)_3]\cdot 4H_2O$	375	11-200	1.84[a]	70	15
			0.2[d]	90	

tba: thiobenzoate; phen: phenantroline; acac $^-$= acetylacetonate; PyAm = 2-amidinopyridine; PmAm= 2-amidinopyrimidine; 4-OHpy = 4-hydroxypyridine; bpm = 2,2'-bipyrimidine; tfaa$^-$= 1,1,1-trifluoroacetylacetonate; $bpyO_2$ = 2,2'-bipiridynedi-N-oxide.

[a] Δ based on the intensity ratio between two Stark transitions ascribed to the $^4F_{9/2} \rightarrow {}^6H_{13/2}$ Dy^{III} transition.

[b] Δ based on the integrated intensity ratio between two spectral ranges of $^4F_{9/2} \rightarrow {}^6H_{15/2}$ Dy^{III} transition.

[c] Δ based on the integrated intensity ratio between the ligand ($T_1 \rightarrow S_0$) and Dy^{III} ($^4F_{9/2} \rightarrow {}^6H_{13/2}$) related emission bands.

[d] Δ based on the ratio between the intensity ratio of two Stark transitions ascribed to the $^4F_{9/2} \rightarrow {}^6H_{15/2}$ Dy^{III} transition.

temperature. The inset of Fig. 7a supports the operative range of **1**·CH_3OH as a luminescent thermometer in the whole temperature range.

The thermal performance of **1**·CH_3OH was evaluated through S_r and δT, which are the figures of merit to characterize the performance of an optical temperature sensor.[23] Fig. 7b illustrates the evolution with the temperature of S_r that increases with the temperature, reaching a maximum value of 1.6%·K^{-1} with a minimum temperature uncertainty δT (see Table S4 for more details) of 1.1 K at 295 K (see Fig. 7c. It is worth mentioning that for temperatures above 295 K the estimation of Δ would be dramatically hindered due to the negligible I_2 values. Then, the abovementioned ratiometric approach will not be suitable for T > 295 K and therefore the extension of the thermal sensing range towards higher temperatures will require the consideration of other thermometric parameters (no analysed in this work), for instance, the full width at half maximum (FHWM) and energy position of the ligand related emission broadband, for instance.

The thermometric performance demonstrated by different reported Dy^{III}-based SMM optical thermometers and **1**·CH_3OH are recorded in Table 1, showing comparable results. It is worth mentioning that there are few examples of Dy^{III}-based SMM optical thermometers in the literature, and mostly of these examples based their luminescent thermometric features on solely Dy^{III} emissions.[7b,11,12,14,17] Our system accesses the thermometric characteristics involving the ligand ascribed to the triplet emission in combination with Dy^{III} emission and, to the best of our knowledge, there is only one example in the literature that shares this feature.[7b] As can be seen in Table 1, this related compound is a dinuclear dysprosium complex, and, although the number of homodi- or polynuclear dysprosium SMMs is very low (only two examples), the data may suggest that this phenomenon is more favoured in SMMs with more than one Dy^{III} ion than in SIMs of the same metal.

Conclusions

The new linear tetranuclear Dy^{III} complex $[Dy_4(1,1,4\text{-}H_3L^r)_2(OAc)_6]\cdot CH_3OH$ (**1**·CH_3OH), which contains two types of octacoordinated Dy^{III} ions, in distorted triangular dodecahedral and square antiprim environments, is a SMM with an anisotropic energy barrier U_{eff} of 39.7 K. In addition, **1**·CH_3OH shows temperature-dependent luminescence and, thus, is the first homonuclear Dy_4 SMM that can also act as a luminescent thermometer. Besides, the origin of this thermometric character is uncommon among the reporter dysprosium SMM thermometers, given that the thermometric characteristics are accessed combining the ligand triplet emission and Dy^{III} intra-4f transitions. Accordingly, this complex contributes to strengthen the pathways through which SMMs can in turn act as luminescent thermometers.

Conflicts of interest

There are no conflicts to declare.

Acknowledgements

Authors thank the Spanish Ministerio de Innovación, Ciencia y Universidades (PGC2018 102052-B-C21), and Xunta de Galicia for financial support. J.C.V also thanks Xunta de Galicia for his postdoctoral fellowship. This work was also developed within the scope of the project CICECO-Aveiro Institute of Materials, UIDB/50011/2020, UIDP/50011/2020 & LA/P/0006/2020, financed by Portuguese funds through the FCT/MEC (PIDDAC).

References

1. E. Coronado, *Nat. Rev. Mater.*, 2020, **5**, 87–104.
2. A. Zabala-Lekuona, J. M. Seco and E. Colacio, *Coord. Chem. Rev.*, 2021, **441**, 213984.
3. J. D. Rinehart and J. R. Long, *Chem. Sci.*, 2011, **2**, 2078–2085.
4. (a) F-S. Guo, B. M. Day, Y-C. Chen, M-L. Tong, A. Mansikkam-ki and R. A. Layfield, *Angew. Chem. Int. Ed.*, 2017, **56**, 11445–11449. (b) C. A. P. Goodwin, F. Ortu, D. Reta, N. F. Chilton and D. P. Mills, *Nature*, 2017, **548**, 439–442.
5. F-S. Guo, B. M. Day, Y-C. Chen, M-L. Tong, A. Mansikkam-ki and R. A. Layfield, *Science*, 2018, **362**, 1400-1403.
6. C. A. Gould, K. R. McClain, D. Reta, J. G. C. Kragskow, D. A. Marchiori, E. Lachman, E-S. Choi, J. G. Analytis, R. D. Britt, N. F. Chilton, B. G. Harvey and J. R. Long, *Science*, 2022, **375**, 198–202.
7. (a) G. Brunet, R. Marin, M-J. Monk, U. Resch-Genger, D. A. Galich, F. A. Sigoli, E. A. Suturina, E. Hemmer and M. Murugesu, *Chem. Sci.*,

2019, **10**, 6799-6808; (b) D. Errulat, R. Marin, D. A. Gálico, K. L. M. Harriman, A. Pialat, B. Gabidullin, F. Iikawa, O. D. D. Couto, Jr., J. O. Moilanen, E. Hemmer, F. A. Sigoli and M. Murugesu, *ACS Cent. Sci*., 2019, **5**, 1187−1198; (c) D. A. Gálico, R. Marin, G. Brunet, D. Errulat, E. Hemmer, F. A. Sigoli, J. O. Moilanen and M. Murugesu, *Chem. Eur. J*., 2019, **25**, 14625–14637.

8. K. Kumar, D. Abe, K. Komori-Orisaku, O. Stefanczyk, K. Nakabayashi, J. R. Shakirova, S. P. Tunik and S. Ohkoshi, *RSC Adv*., 2019, **9**, 23444–23449.

9. J. Wang, J. J. Zakrzewski, M. Heczko, M. Zychowicz, K. Nakagawa, K. Nakabayashi, B. Sieklucka, S. Chorazy and S. Ohkoshi, *J. Am. Chem. Soc*., 2020, **142**, 3970−3979.

10. M. Fondo, J. Corredoira-Vázquez, A. M. García-Deibe, J. Sanmartín-Matalobos, M. Amoza, A. M. P. Botas, R. A. S. Ferreira, L. D. Carlos, E. Colacio, *Inorg. Chem. Front*., 2020, **7**, 3019-3029.

11. A. A. Kitos, D. A. Gálico, N. Mavragani, R. Castañeda, J. O. Moilanen, J. L. Brusso and M. Murugesu, *Chem. Commun.*, 2021, ***57***, 7818–7821.

12. R. A. S. Ferreira, E. Mamontova, A. M. P. Botas, M. Shestakov, J. Vanacken, V. Moshchalkov, Y. Guari, L. F. Chibotaru, D. Luneau, P. S. André, J. Larionova, J. Long and L. D. Carlos, *Adv. Optical Mater*., 2021, **9**, 2101495.

13. K. Kumar, O. Stefanczyk, K. Nakabayashi, K. Imoto, Y. Oki and S-i. Ohkoshi, *Adv. Optical Mater*., 2022, **10**, 2101721.

14. K. Karachousos-Spiliotakopoulos, V. Tangoulis, N. Panagiotou, A. Tasiopoulos, E. Moreno-Pineda, W. Wernsdorfer, M. Schulze, A. M. P. Botas and L. D. Carlos, *Dalton Trans*., 2022, **51**, 8208–8216.

15. V. Tangoulis, V. Nastopoulos, N. Panagiotou, A. Tasiopoulos, G. Itskos, M. Athanasiou, E. Moreno-Pineda, W. Wernsdorfer, M. Schulze and O. Malina, *Inorg. Chem*., 2022, **61**, 2546−2557.

16. J. Wang, J. J. Zakrzewski, M. Zychowicz, V. Vieru, L. F. Chibotaru, K. Nakabayashi, S. Chorazy and S-i. Ohkoshi, *Chem. Sci*., 2021,**12**, 730-741.

17. R. Marin, D. A. Gálico, R. Gayfullina, J. O. Moilanen, L. D. Carlos, D. Jaque and M. Murugesu, *J. Mater. Chem. C*, 2022, Advance Article.

18. R. Marin, G. Brunet and M. Murugesu, *Angew. Chem. Int. Ed.*, 2021, **60**, 1728–1746.

19. (a) M. Fondo, A. M. García-Deibe, M. R. Bermejo, J. Sanmartín and A. L. Llamas-Saiz, *J. Chem. Soc., Dalton Trans*., 2002, 4746-4750; (b) M. Fondo, N. Ocampo, A. M. García-Deibe, E. Ruiz, J. Tercero, J. Sanmartín, *Inorg. Chem*., 2009, **48**, 9861–9873.

20. L.-W. Yang, S. Liu, E. Wong, S. J. Rettig and C. Orvig, *Inorg. Chem*., 1995, **34**, 2164-2178.

21. G. M. Sheldrick, *SADABS, Area-Detector Absorption Correction*; Siemens Industrial Automation, Inc.: Madison, WI, 2001.

22. G. M. Sheldrick, *Acta Cryst.*, 2015, **C71**, 3–8.

23. C. D. S. Brites, S. Balabhadra and L. D. Carlos, *Adv.Optical Mater.*, 2019, ***7***, 1801239.

24. M. Fondo, J. Corredoira-Vázquez, A. M. García-Deibe, J Sanmartín-Matalobos, S. Gómez-Coca and E. Ruiz, Colacio, *Inorg. Chem. Front*., 2021, **8**, 2532–2541.

25. (a) M. Llunell, D. Casanova, J. Cirera, J. M. Bofill, P. Alemany, S. Alvarez, M. Pinsky and D. D. Avnir, SHAPE v1.1b, Barcelona, 2005; (b) A. Ruiz-Martínez, D. Casanova and S. Alvarez, Chem. Eur. J., 2008, **14**, 1291–1303; (c) M. Llunell, D. Casanova, J. Cirera, P. Alemany and S. Alvarez, SHAPE: Program for the stereochemical analysis of molecular fragments by means of continuous shape measures and associated tools; University of Barcelona, Barcelona, Spain, 2010.

26. M. Fondo, J. Corredoira-Vázquez, A. M. García-Deibe, J Sanmartín-Matalobos, D. Reta and E. Colacio, *Dalton Trans*, 2021, **50**, 15878-15887.

27. S. She, G. Su, B. Wang, Q. Lei, Y. Yang, L. Gong and B. Liu, *Eur. J. Inorg. Chem*., 2017, 2406–2412.

28. M. Guo, Y. Xu, J. Wu, L. Zhao and J. Tang, *Dalton Trans*., 2017, **46**, 8252-8258.

29. J-L. Liu, Y-C. Chen and M-L. Tong, *Chem. Soc. Rev*., 2018, **47**, 2431—2453.

30. (a) A. Singh and K. N. Shrivastava, Optical-acoustic two-phonon relaxation in spin systems, *Phys. Status Solidi* B, 1979, **95**, 273-277; (b) K. N. Shrivastava, Theory of spin–lattice relaxation, *Phys. Status Solidi* B, 1983, **117**, 437-458.

31. H. Ke, G-F. Xu, Y-N. Guo, P. Gamez, C. M. Beavers, S. J. Teat and J. Tang, *Chem. Commun*., 2010, **46**, 6057–6059.

32. B. H- Koo, K. S. Lim, D. W. Ryu, W. R. Lee, E, K, Koh and C. S. Hong, *Dalton Trans*., 2013, **42**, 7204–7209.

33. M. Yadav, A. Mondal, V. Mereacre, S. K. Jana, A. K. Powell and P. W. Roesky, *Inorg. Chem*., 2015, **54**, 7846−7856.

34. J. Acharya, S. Biswas, J. van Leusen, P. Kumar, V. Kumar, R. S. Narayanan, P. Kögerler and V. Chandrasekhar, *Cryst. Growth Des*., 2018, **18**, 4004−4016.

35. Y. Yu, J. Zhang, J-H. Zhao and K. Ren, *Polyhedron*, 2020, **192**, 114830

36. Y-N. Guo, G-F. Xu, P. Gamez, L. Zhao, S-Y. Lin, R. Deng, J. Tang and H-J. Zhang, *J. Am. Chem. Soc*., 2010, **132**, 8538–8539.

37. L. C. Thompson, J. R. Marvin and N. C. Bettenberg, *J. Alloys Compd*, 1992*,* **180***,* 229–234.

38. C. Molina, R. A. S. Ferreira, G. Poirier, L. Fu, S. J. L. Ribeiro, Y. Messsaddeq and L. D. Carlos, *J. Phys. Chem. C*, 2008*,* **112***,* 19346–19352.

39. J. Kimball, J. Chavez, L. Ceresa, E. Kitchner, Z. Nurekeyev, H. Doan, M. Szabelski, J. Borejdo, I. Gryczynski and Z. Gryczynski, *Methods Appl. Fluoresc.,* 2020, **8**, 033002.